ADVANCED FUNCTIONAL MATERIALS

Supporting Information

for *Adv. Funct. Mater.,* DOI: 10.1002/adfm.201807767

Bulk Photodriven CO_2 Conversion through TiO_2@Si(HIPE) Monolithic Macrocellular Foams

Sophie Bernadet, Eugénie Tavernier, Duc-Minh Ta, Renaud A. L. Vallée, Serge Ravaine, Antoine Fécant,* and Rénal Backov**

Supporting Information

Bulk Photo-Driven CO_2 Conversion through TiO_2@Si(HIPE) Monolithic Macrocellular Foams

Sophie Bernadet[1,2], Eugénie Tavernier[2], Duc-Minh Ta[1], Renaud A. L. Vallée[1], Serge Ravaine[1,*], Antoine Fécant[2,*] and Rénal Backov[1,3,*]

Correspondence to: ravaine@crpp-bordeaux.cnrs.fr; antoine.fecant@ifpen.fr; backov@crpp-bordeaux.cnrs.fr; backov@mit.edu

This PDF file includes:

Section 1: Photonic investigations

Photonic apparatus

Simultaneous spatial and time-resolved setup is consisting of a streak camera (HAMAMATSU Streak Scope C10627). The excitation light was the frequency doubled output of the λ = 1030 nm wavelength, 10 MHz repetition rate, 300 fs line width pulses delivered by a diode-pumped Ytterbium femtosecond oscillator from Amplitude systems (t-Pulse 200). The beam was very slightly focused to a 1 mW, 1 mm spot diameter on the slab; the transmission intensity was focused on the entrance slit of the camera.

Photonic simulation

The full solution of the diffusion equation writes as:

$$T(t) = \frac{e^{-\frac{Dt}{l_i^2}}}{4t(4\pi Dt)^{\frac{3}{2}}} \sum_{j=-\infty}^{j=+\infty} \left(A e^{-\frac{A^2}{4Dt}} - B e^{-\frac{B^2}{4Dt}} \right), \quad \text{S1}$$

With:

$$A = (1-2j)(L+2z_e) - 2\left(z_p + l_t\right) \quad \text{S2}$$

$$B = (2j+1)(L+2z_e) \quad \text{S3}$$

$$D = \frac{c l_t}{3n} \quad \text{S4}$$

$$z_e = \frac{l_i}{2} \ln\left(\frac{1+\frac{z_0}{l_i}}{1-\frac{z_0}{l_i}}\right) \quad \text{S5}$$

where T(t), D, l_i, z_p, z_e, c and n feature the forward transmission, the diffusion constant, the inelastic absorption length, the penetration length, the extrapolation length, the speed of light and the refractive index in the medium, respectively.

In the Table S5, results for all photonic simulation are provided.

Section 2: Photocatalytic methodology

Photocatalytic experiments were carried out in continuous in a stainless steel fixed bed reactor gas flow passing through the sample, operating at atmospheric pressure and ambient temperature. CO_2/H_2O molar ratio (obtained by CO_2 bubbling in water tank, Fig. S4) was fixed at 30 and CO_2 gas flow was fixed at 0.3 cc.min^{-1}. Irradiance for 315-400 nm wavelength range was adjusted to 80 W.m^{-2} and controlled with a radiometer equipped with CCD captor (Delta Ohm), corresponding to a Photon Flux Density (PFD) of $2.62.10^{-4}$ mol. s^{-1}.m^{-2}, and provided by a Xe lamp Max303 Asahi (irradiance spectra Fig. S7). Moreover, the reactor had an optical quartz window through which the light flux reaches the material (Fig. S5). Prior to insert the monolith in the reactor, it is slightly sanded to homogenize and flatten the surface that will be irradiated with silicon carbide grinding disc (grit size 500, Buehler). Then, the TiO_2@Si(HIPE)s thickness is adjusted from one test to the next using this silicon carbide grinding disc, and measured using a caliper rule with an accuracy of 0.1 mm. This one was supported on a Teflon ring, joined by a line of vacuum grease (Fig. S6). Reagents and products were then analyzed on-line by a gas chromatograph TCD sensor microchromatograph Lan3000 (SRA Instruments, µGC-TCD). Gas phase analyses were performed every 10 minutes. The analytical parameters selected for optimal gas separation under our conditions are presented in Table S6. The micro-chromatograph was calibrated for all gases from different gas cylinders with controlled contents purchased from Air Liquide. The retention times, in seconds, of the gases analyzed by the first three columns of the chromatograph are listed in Table S7. No species produced has been detected on the fourth one, retention times will not be itemized.

According to the simplified reaction equation (Eq S6, all products and reactants in the gas phase, unbalanced for clarity reason), a couple of products could be produced. Then, to evaluate the photocatalytic performances of materials for CO_2 reduction, the calculated parameters have to take into account all products. Two parameters are then defined: average electron consumption rate (Eq S8) and average selectivity (Eq S9), and calculated after 20 hours on stream (T.O.S.).

$$CO_2 + H_2O + h\nu \rightarrow O_2 + H_2, CO, CH_4, C_2H_6, C_3H_8 \ldots \quad \text{S6}$$

$$\overline{r^{e^-}_{\begin{cases} S \\ m \end{cases}}} = \frac{1}{T.O.S.} \int_0^{T.O.S.} \sum_i \frac{n_i^{e^-} * [i](t) * Q_{tot}}{V_m^{25°C} * \begin{cases} S_{irradiated} \\ m_{catalyst} \end{cases}} * 60 \; dt \quad \text{S7}$$

$$\overline{S_i^{H^+}} = \frac{1}{T.O.S.} \int_0^{T.O.S.} \frac{n_i^{H^+} * [i](t)}{\sum_j n_j^{H^+} * [j]\,(t)} \; dt \quad \text{S8}$$

Where, $n^{\begin{cases} e^- \\ H^+ \end{cases}}_{\begin{cases} i \\ j \end{cases}}$ is the stoichiometric coefficient of the electrons (or protons) consumed by the product i (or j) (e.g. 2 e$^-$ is needed to form H_2 or CO, whereas CH_4 needs 8), $\left[\begin{cases} i \\ j \end{cases}\right](t)$ is the concentration of product i (or j) over time (in ppmVol), Q_{tot} is CO_2 and H_2O input flow rate ($3.09 \cdot 10^{-4} L.\min^{-1}$),and $V_m^{25°C}$ is the molar volume of a gas at 25°C (24.5 L.mol^{-1}). Actually, two types of electron consumption rate could be distinguished: one intrinsic (normalized by the

catalyst mass), and the other global (normalized by the irradiated section, $S^{irr}_{monolith} = 8.04 * 10^{-4}\ m^2, S^{irr}_{powder} = 5.31 * 10^{-4}\ m^2$). Both give complementary information. The first one provides information on intrinsic performances of the catalyst, closely related to the crystalline structure of this catalyst and limited by photon intake, and the second one reveals global performance related to irradiated area. In addition, the proton selectivity evaluates the overall orientation of the reactions towards the formation of desired products compared to the (undesired) dihydrogen, resulting from the recombination of the protons generated by water oxidation.

Average electron consumptions are given with a standard deviation of ± 10% relative. Prior to photocatalytic evaluation of materials, a test has been carried out with empty reactor without detection of any products aforementioned. Also, TiO_2 powder and TiO_2@Si(HIPE)s have been tested with Argon replacing CO_2 gas, thus only water vapor is fed to the reactor, and no carbon containing products have been detected, only H_2 coming from water splitting.

For visualization convenience, we propose two examples of classical photocatalytic test following-up in Fig. S8, showing instantaneous rates of H_2, CO, CH_4, and C_2H_6 production versus time on stream.

Section 3: Kinetic modelling

We describe below the main reactions or semi-reactions involving in one hand photo-generated electrons and holes, and in another hand all the gas phase compounds measured during experimentation (meaning H_2O, CO_2, H_2, CO, CH_4, C_2H_6 and O_2).

e^-/h^+ pairs generation:

$$h\nu \xrightarrow[k_0]{TiO_2} h^+ + e^- \quad \text{S9}$$

overall water splitting and CO_2 reduction main semi-reactions:

$$e^- + H^+ \xrightarrow[k_1]{TiO_2} \frac{1}{2}H_2 \quad \text{S10}$$

$$e^- + H^+ + \frac{1}{2}CO_2 \xrightarrow[k_1']{TiO_2} \frac{1}{2}CO + \frac{1}{2}H_2O \quad \text{S11}$$

$$e^- + H^+ + \frac{1}{8}CO_2 \xrightarrow[k_1'']{TiO_2} \frac{1}{8}CH_4 + \frac{1}{4}H_2O \quad \text{S12}$$

$$e^- + H^+ + \frac{1}{7}CO_2 \xrightarrow[k_1''']{TiO_2} \frac{1}{14}C_2H_6 + \frac{2}{7}H_2O \quad \text{S13}$$

$$h^+ + \frac{1}{2}H_2O \xrightarrow[k_2]{TiO_2} H^+ + \frac{1}{4}O_2 \quad \text{S14}$$

main reverse semi-reactions:

$$h^+ + \frac{1}{2}H_2 \xrightarrow[k_{-1}]{TiO_2} H^+ \quad \text{S15}$$

$$h^+ + \frac{1}{2}CO + \frac{1}{2}H_2O \xrightarrow[k_{-1}']{TiO_2} H^+ + \frac{1}{2}CO_2 \quad \text{S16}$$

$$h^+ + \frac{1}{8}CH_4 + \frac{1}{4}H_2O \xrightarrow[k_{-1}'']{TiO_2} H^+ + \frac{1}{8}CO_2 \quad \text{S17}$$

$$h^+ + \frac{1}{14}C_2H_6 + \frac{2}{7}H_2O \xrightarrow[k_{-1}''']{TiO_2} H^+ + \frac{1}{7}CO_2 \quad \text{S18}$$

$$e^- + H^+ + \frac{1}{4}O_2 \xrightarrow[k_{-2}]{TiO_2} \frac{1}{2}H_2O \quad \text{S19}$$

Thus, rate equations involving electrons consumption or generation can be written considering the following assumptions:

- surface reactions are the limiting step (compared to adsorption)
- a Langmuir-Hinshelwood formalism is applied; except for photons because they are mostly supposed to be absorbed in the bulk of TiO_2 nanoparticles
- stoichiometric coefficients are equal to the partial orders, as each reaction is bethought as elementary step; except for CO_2 and H_2O. For them, a 0 order is assumed due to their concentration which not significantly change in and out of the reactor (large excess):

$$r_{e^-}^{hv}(h) = k_0 . E(h) . C_s^{irr}(h) \quad \text{S20}$$

$$r_{e^-}^{H2}(h) = k_1 . n_{H+}^{surf\,1} . n_{e^-}^{surf\,1} = K_1 . \theta_{H+} . \theta_{e^-} . C_s^{irr}(h)^2 \quad \text{S21}$$

$$r_{e^-}^{CO}(h) = k_1' . n_{H+}^{surf\,1} . n_{e^-}^{surf\,1} . n_{CO2}^{surf\,0} = K_1' . \theta_{H+} . \theta_{e^-} . C_s^{irr}(h)^2 \quad \text{S22}$$

$$r_{e^-}^{CH4}(h) = k_1'' . n_{H+}^{surf\,1} . n_{e^-}^{surf\,1} . n_{CO2}^{surf\,0} = K_1'' . \theta_{H+} . \theta_{e^-} . C_s^{irr}(h)^2 \quad \text{S23}$$

$$r_{e^-}^{C2H6}(h) = k_1''' . n_{H+}^{surf\,1} . n_{e^-}^{surf\,1} . n_{CO2}^{surf\,0} = K_1''' . \theta_{H+} . \theta_{e^-} . C_s^{irr}(h)^2 \quad \text{S24}$$

$$r_{e^-}^{O2}(h) = k_{-2} . n_{H+}^{surf\,1} . n_{e^-}^{surf\,1} . n_{O2}^{surf\,1/4} = k_{-2} . \theta_{H+} . \theta_{e^-} . \theta_{O2}{}^{1/4} . C_s^{irr}(h)^{9/4} \quad \text{S25}$$

$r_{e^-}^{hv}(h)$ being the rate of electron generation from photon absorption by TiO_2. $r_{e^-}^{H2}(h)$, $r_{e^-}^{CO}(h)$, $r_{e^-}^{CH4}(h)$, $r_{e^-}^{C2H6}(h)$ being the rates of electrons consumption for H_2, CO, CH_4 and C_2H_6 production respectively. $r_{e^-}^{O2}(h)$ being the rate of electrons consumption for O_2 back reduction. All rates are expressed in (mol.h^{-1}) and reported as a function of h, being the photocatalytic bed thickness in (m). K_1, K_1', K_1'' and K_1''' are apparent kinetic constants in (mol^{-1}.h^{-1}). k_0 and k_{-2} being kinetic constants in (mol^{-1}.h^{-1}) and (mol$^{-5/4}$.h^{-1}) respectively. n_X^{surf} being the amount of specie X onto the TiO_2 surface in (mol), θ_X being the surface coverage onto TiO_2 nanoparticles for each species X.

$E(h)$ is defined as the molar quantity in (mol) of absorbable photons (315-400 nm, corresponding to a bandgap of 3.1 eV) within the bed thickness h, expressed as below considering light scattering is following Beer-Lambert law :

$$E(h) = E^0 \times \int_0^h e^{-\alpha . z} . dz = E^0 \times \frac{(1 - e^{-\alpha h})}{\alpha} \quad \text{S26}$$

α being an attenuation coefficient related to the Beer-Lambert law in (m^{-1}), z the position between 0 and h in the depth axis of photocatalyst bed, and E^0 being the molar quantity in absorbable photons (315-400 nm) per unit of depth without attenuation (mol.m^{-1}), being expressed as followed :

$$E^0 = \frac{PFD.S^{irr}}{v}$$

S27

PFD being the Photon Flux Density and set at $2.62.10^{-4}$ mol.s^{-1}.m^{-2} for each experiment, S^{irr} being the geometric irradiated section of the material, and v being the velocity of light in the photcatalytic bed in (m.s^{-1}) and expressed as followed:

$$v = \frac{\varepsilon.c}{n_{air}} + \frac{(\varepsilon - 1).\%_{TiO2}^{m}.c}{n_{TiO2}.\left(\%_{TiO2}^{m} + \%_{SiO2}^{m} \times \frac{d_{TiO2}}{d_{SiO2}}\right)} + \frac{(\varepsilon - 1).\%_{SiO2}^{m}.c}{n_{SiO2}.\left(\%_{SiO2}^{m} + \%_{TiO2}^{m} \times \frac{d_{SiO2}}{d_{TiO2}}\right)}$$

S28

ε being the porosity of the bed or monolith, c being the celerity of light in vaccum (299 792 458 m.s^{-1}), n_{air} being the refractive index of air (1.0003), n_{TiO2} being the refractive index of TiO_2 (2.61), n_{SiO2} being the refractive index of SiO_2 (1.45), $\%_{TiO2}^{m}$ being the mass percentage of TiO_2 in the sample, $\%_{SiO2}^{m}$ being the mass percentage of SiO_2 in the sample, d_{TiO2} being the density of TiO_2 (4.23 kg.L^{-1}), d_{SiO2} being the density of SiO_2 (2.65 kg.L^{-1}).

${C_s}^{irr}(h)$ is defined by the molar quantity of irradiated TiO_2 surface sites and can be expressed as followed:

$${C_s}^{irr}(h) = C_s \times \int_0^h e^{-\alpha.z}.dz = C_s \times \frac{(1 - e^{-\alpha h})}{\alpha}$$

S29

C_s being molar quantity of TiO_2 surface sites per unit of depth (mol.m^{-1}), being expressed as followed:

$$C_s = \frac{d_{sample}.S^{irr}.10^6.\%_{TiO2}^{m}.D_{TiO2}}{M_{TiO2}}$$

S30

d_{sample} being the bulk density of powder bed or TiO_2@Si(HIPE) in g.mL^{-1}, M_{TiO2} being the molar mass of TiO_2 (80 g.mol^{-1}), and D_{TiO2} the dispersion of tetrahedral TiO_2 cluster assuming a spherical model. D_{TiO2} is expressed as followed:

$$D_{TiO2} = \frac{6.V_{TiO2}}{S_{TiO2}.d_{part}}$$

S31

V_{TiO2} being the volume of equivalent sphere for tetrahedral TiO_2 cluster (0.034205 nm^3), S_{TiO2} being the section of equivalent sphere for tetrahedral TiO_2 cluster (0.127394 nm^2). V_{TiO2} and S_{TiO2} are calculated using crystallographic data for anatase TiO_2 given in Material Studio 7.0

software by Accelerys ®. d_{part} being the TiO_2 mean diameter in nm, given by XRD analysis using Scherrer equation.

Having defined each terms or equation rate, and considering electron as a very reactive intermediate, thus we applied for this specie steady state approximation, meaning:

$$\frac{d\theta_{e-}}{dt} = 0 = r_{e-}^{hv}(h) - r_{e-}^{H2}(h) - r_{e-}^{CO}(h) - r_{e-}^{CH4}(h) - r_{e-}^{C2H6}(h) - r_{e-}^{O2}(h) \quad \text{S32}$$

Thus

$$\begin{aligned} 0 = k_0.E(h).C_s^{irr}(h) - K_1.\theta_{H+}.\theta_{e-}.C_s^{irr}(h)^2 - K_1'.\theta_{H+}.\theta_{e-}.C_s^{irr}(h)^2 \\ - K_1''.\theta_{H+}.\theta_{e-}.C_s^{irr}(h)^2 - K_1'''.\theta_{H+}.\theta_{e-}.C_s^{irr}(h)^2 \\ - k_{-2}.\theta_{H+}.\theta_{e-}.{\theta_{O2}}^{1/4}.C_s^{irr}(h)^{9/4} \end{aligned} \quad \text{S33}$$

And

$$\theta_{e-} = \frac{k_0.E(h).C_s^{irr}(h)}{K_1.\theta_{H+}.C_s^{irr}(h)^2 + K_1'.\theta_{H+}.C_s^{irr}(h)^2 + K_1''.\theta_{H+}.C_s^{irr}(h)^2 + K_1'''.\theta_{H+}.C_s^{irr}(h)^2 + k_{-2}.\theta_{H+}.{\theta_{O2}}^{1/4}.C_s^{irr}(h)^{9/4}} \quad \text{S34}$$

As we define the global reaction rate as the sum of electron consumption for H_2, CO, CH_4 and C_2H_6 production, thus we define global reaction rate $r_{e-}(h)$ in mol.h^{-1} as:

$$r_{e-}(h) = r_{e-}^{hv}(h) - r_{e-}^{O2}(h) \quad \text{S35}$$

$$r_{e-}(h) = k_0.E(h).C_s^{irr}(h) - k_{-2}.\theta_{H+}.\theta_{e-}.{\theta_{O2}}^{1/4}.C_s^{irr}(h)^{9/4} \quad \text{S36}$$

By introducing θ_{e-} equality given by steady state approximation, we get:

$$r_{e-}(h) = k_0.E(h).C_s^{irr}(h) \times \frac{(K_1 + K_1' + K_1'' + K_1''')}{(K_1 + K_1' + K_1'' + K_1''') + k_{-2}.{\theta_{O2}}^{1/4}.C_s^{irr}(h)^{1/4}} \quad \text{S37}$$

This equation is then only depending on $E(h)$ and $C_s^{irr}(h)$, which are measurable parameters depending on α, and θ_{O2}, for which it is much more difficult to find relevant description. Nevertheless, we assume a strong dependence between $\theta_{O2}$and $E(h)$ as O_2 is the common co-product of all H^+ and CO_2 photoreduction, then we propose a n order relationship between $\theta_{O2}$and $E(h)$ as follow:

$$\theta_{O2} = K_{O2} \times \frac{E(h)^n}{C_s^{irr}(h)} \quad \text{S38}$$

This assumption allows us to simplify the global rate equation as:

$$\boldsymbol{r_{e-}(h) = k_0 . E(h) . C_s^{irr}(h) \times \frac{K}{K+E(h)^{n/4}}} \quad \text{in mol.h}^{-1}$$

S39

or

$$\boldsymbol{r_{e-}(h) = \frac{k_0 . E(h) . C_s^{irr}(h)}{S^{irr}} \times \frac{K}{K+E(h)^{n/4}}} \quad \text{in mol.h}^{-1}\text{.m}^{-2}$$

S40

With

$$K = \frac{(K_1 + K_1' + K_1'' + K_1''')}{k_{-2} . K_{O2}{}^{1/4}}$$

S41

This global equation rate may then be fitted with the experimental r_{e-} in mol.h^{-1}.m^{-2} defined earlier (Eq. S8):

$$\overline{r_S^{e-}} = \frac{1}{T.O.S.} \int_0^{T.O.S.} \sum_i \frac{n_i^{e^-} * [i](t) * Q_{tot}}{V_m^{25°C} * S^{irr}} * 60 * dt$$

S42

Using least-squares method, when adjusting k_0, K, α and n it has been made possible to best fit model and experimental data for the four samples (one powder bed and the TiO_2@Si(HIPE)s I, II and III) by minimizing the sum of squared residuals :

$$S = \sum_{i=1}^{n} r_i^2, \text{ with } \quad r_i = y_i^{experimental} - y_i^{model}$$

S43

Experimental data are provided in the Table S8. It has been found a unique n order value being 16, and other best fitted parameters are provided in the Table S9

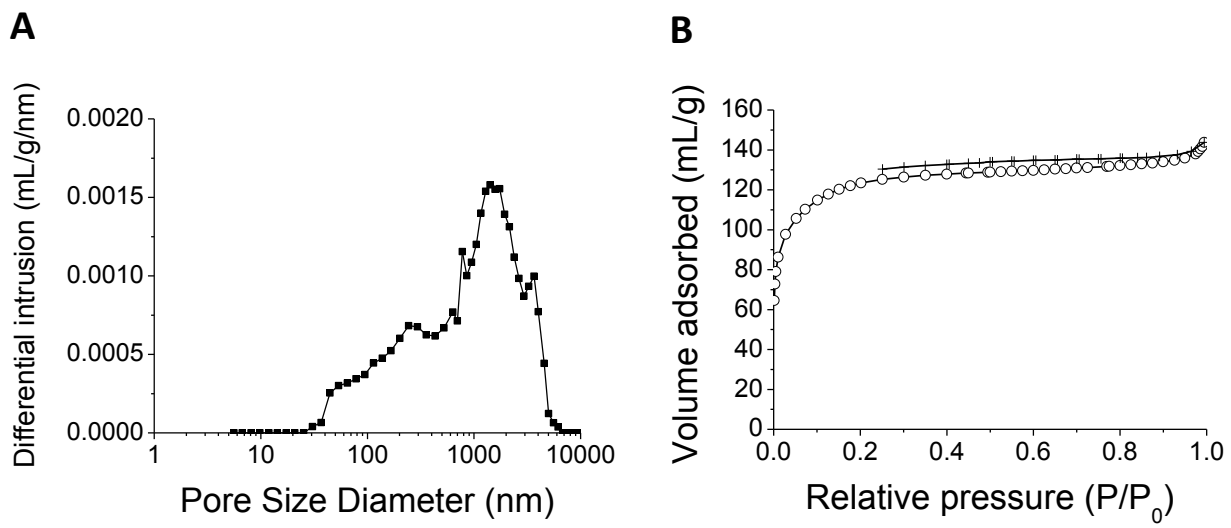

Fig. S1: **Textural characterizations of TiO_2@Si(HIPE) I.** (**A**) Pore size distribution as measured by mercury intrusion porosimetry. (**B**) Nitrogen adsorption (○) and desorption (+) isotherms.

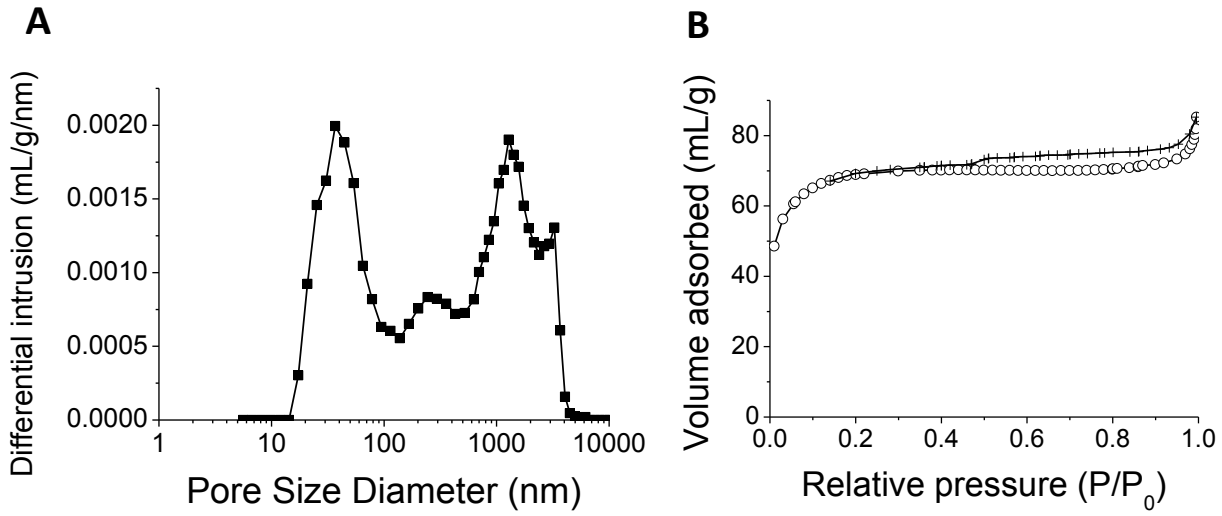

Fig. S2. Textural characterizations of TiO_2@Si(HIPE) II. (**A**) Pore size distribution as measured by mercury intrusion porosimetry. (**B**) Nitrogen adsorption (○) and desorption (+) isotherms.

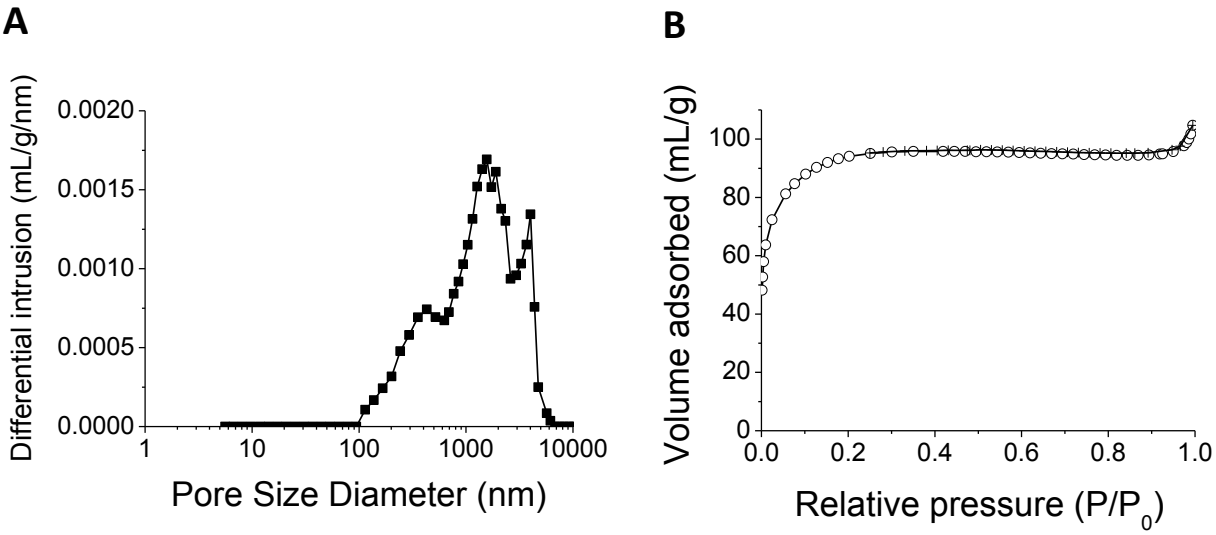

Fig. S3: **Textural characterizations of TiO_2@Si(HIPE) III.** (**A**) Pore size distribution as measured by mercury intrusion porosimetry. (**B**) Nitrogen adsorption (○) and desorption (+) isotherms.

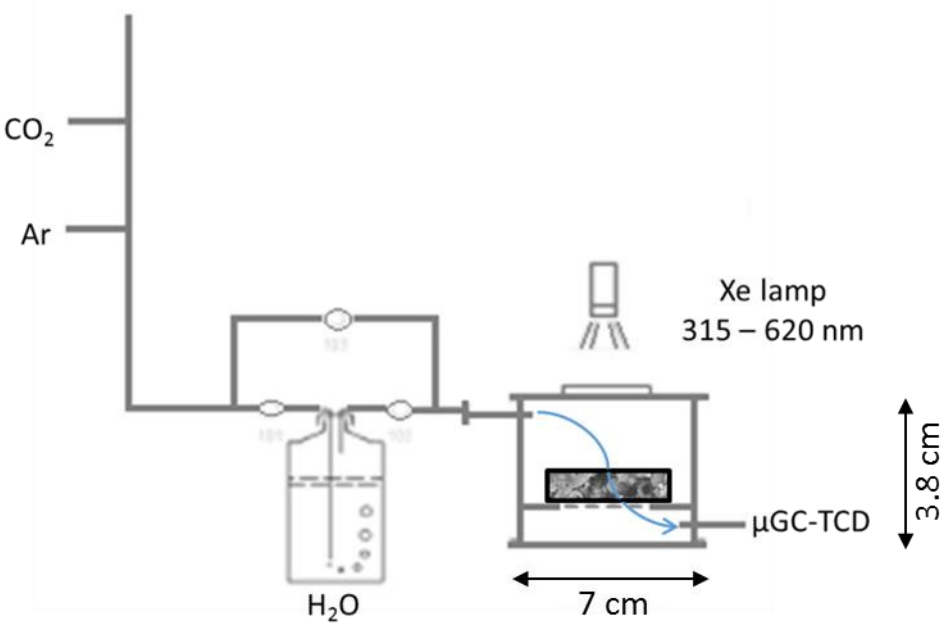

Fig. S4: Schematic representation of photocatalytic experiment set up

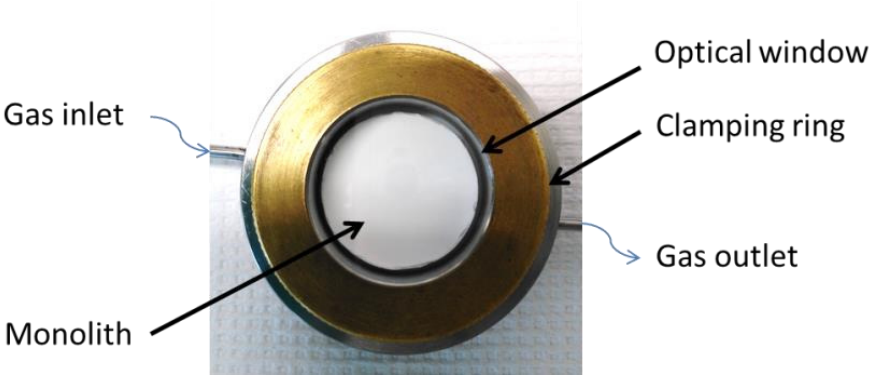

Fig. S5: Top view of the monolith-Teflon ring assembly inside the reactor (for size representation, monolith diameter is 3.2 cm).

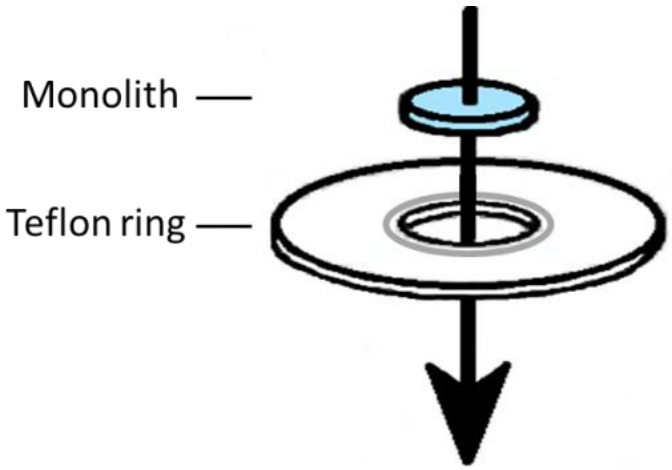

Fig. S6: Schematic representation of the monolith - Teflon ring assembly

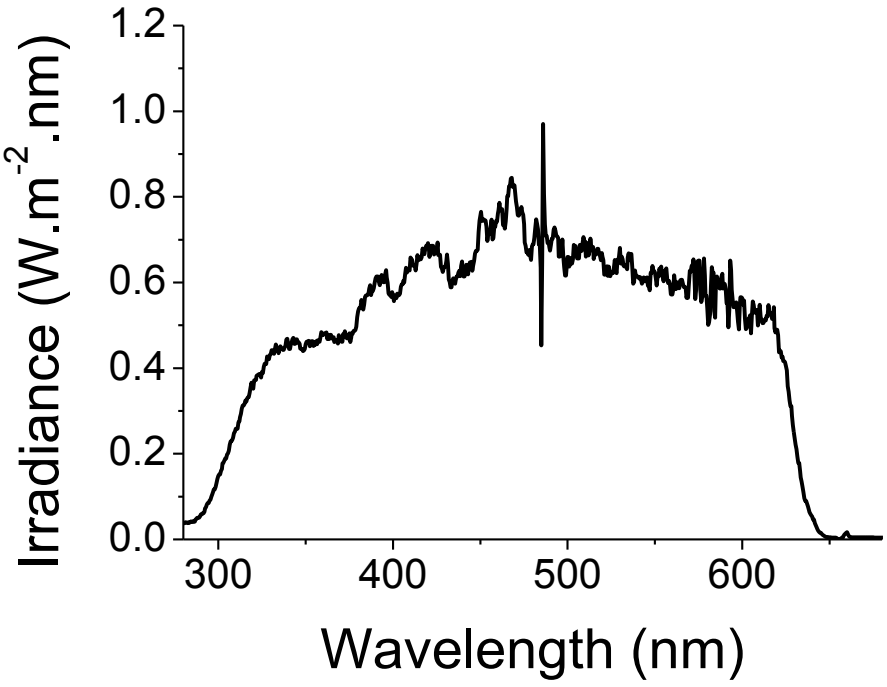

Fig. S7: Irradiance spectra of Max303 Asahi Xenon lamp

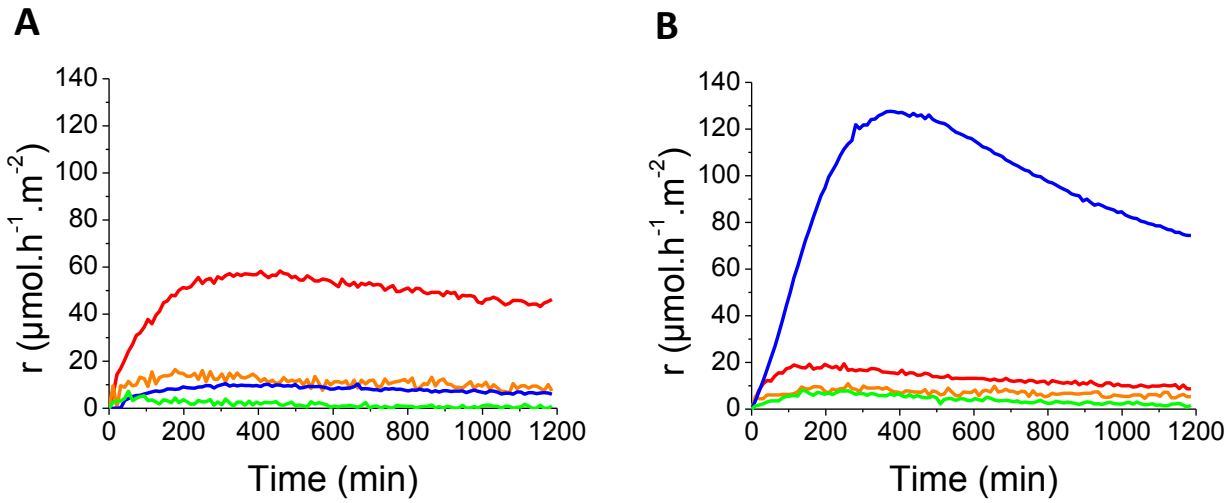

Fig. S8. **Example of photocatalytic tests following production rates as a function of time on stream.** Productions of all products detected are drawn: H_2 (red), CO (orange), CH_4 (blue) and C_2H_6 (green). (**A**) for a 0.65 mm thick TiO_2 powder, and (**B**) for the 2.7 mm thick TiO_2@Si(HIPE) I.

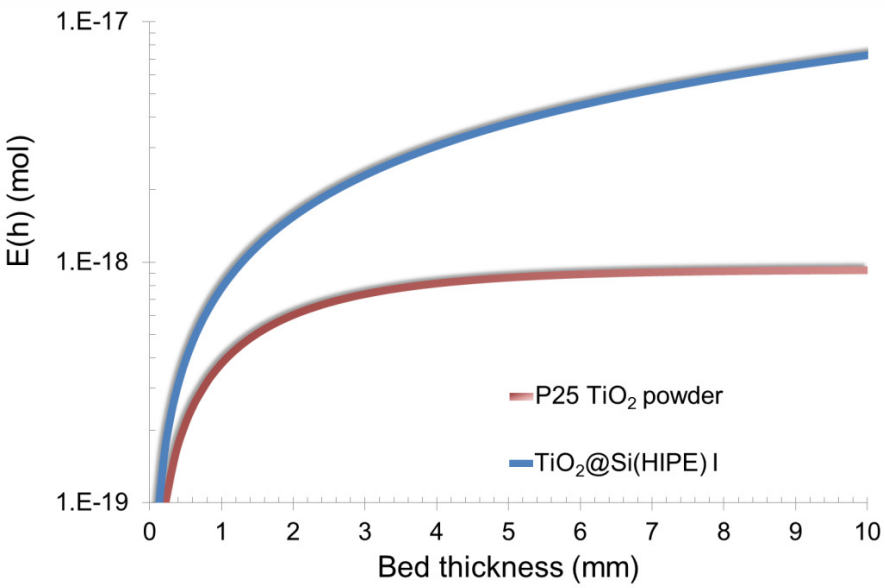

Fig. S9. Profiles of 315-400 nm photon quantity (mol) as a function of bed thickness extracted from α value related to the kinetic model for bed powder and TiO_2@Si(HIPE). Only TiO_2@Si(HIPE) I is represented for clarity reason as their α values are closed compared to powder bed.

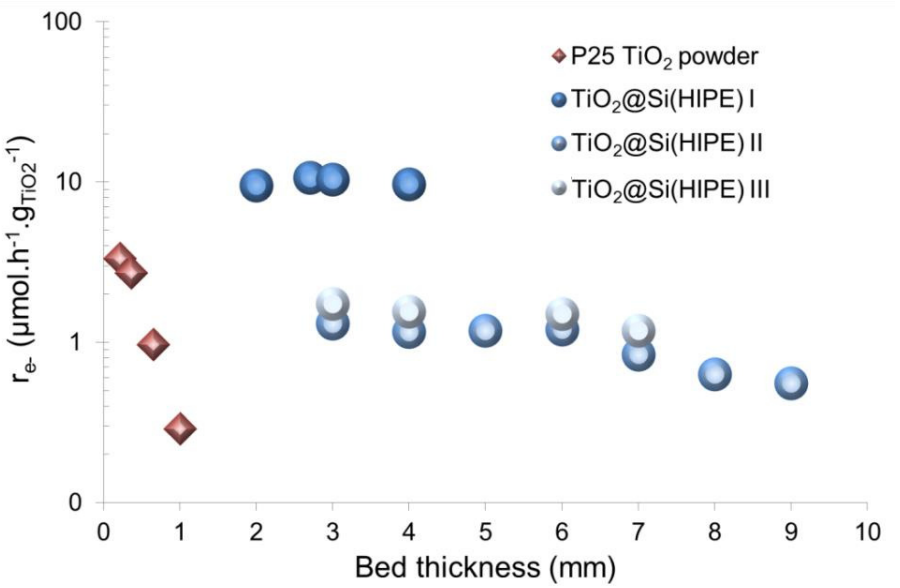

Fig. S10. Global activity per mass of TiO_2 as a function of bed thickness for TiO_2 powder bed and TiO_2@Si(HIPE)s. Because of log scale on y axis, error bars lie within the size of the represented experimental dots given with a relative standard deviation of 10%.

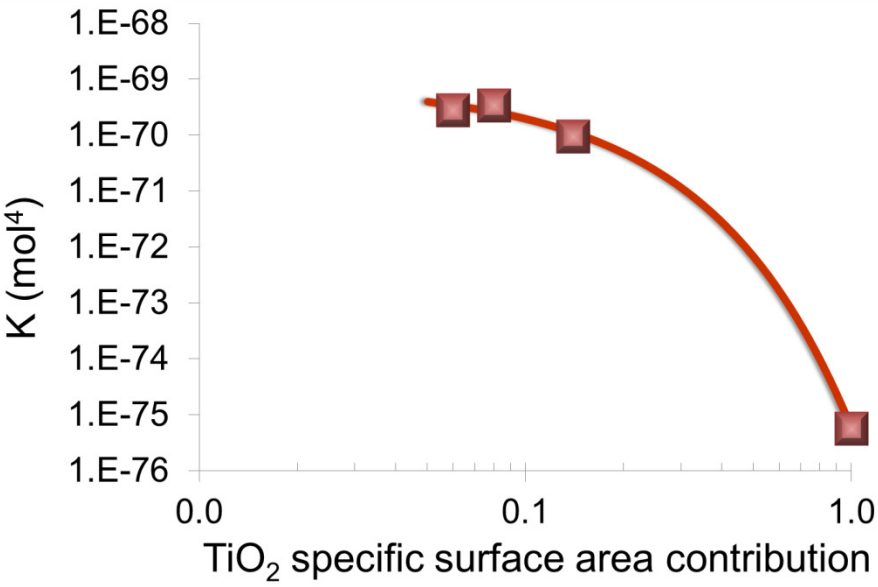

Fig. S11. Observed trend between constant K from kinetic model and the TiO_2 specific surface area contribution. This contribution is calculated using spherical model for TiO_2 particle to get the specific surface associated with TiO_2 nanoparticle with diameter given by XRD, the latter being divided by the global specific area measured by N_2 desorption. The contribution for P25 TiO_2 is 1, meaning that all the specific surface is due to TiO_2 nanoparticle. A specific surface area contribution close to 0 means a high dilution of TiO_2 within the sample. An exponential correlation is observed with a coefficient $R^2 = 0.9989$. Because of log scale on x axis, error bars of TiO_2 specific surface contribution (evaluated at around 15% relative) lie within the size of the represented experimental dots

Materials		TiO_2@Si(HIPE)		
		I	II	III
1st solution	TTIP concentration (M)	0.29	0.29	0.22
	Age (h)	2	2	2
2nd solution	TTIP concentration (M)	0.29	0.29	0.22
	Age (h)	2	38	2

Table S1. Summary table of the differences between the three TiO_2@Si(HIPE)s during impregnation steps

Materials	TiO_2@Si(HIPE)			TiO_2 P25
	I	II	III	Powder
BET surface ($m^2.g^{-1}$)	459	259	350	52
%vol. mesoporous (%)	15	20	10	n.d.

Table S2. Nitrogen physisorption data

Materials	TiO_2@Si(HIPE)			TiO_2 P25
	I	II	III	Powder
Intrusion volume ($mL.g^{-1}$)	6.31	6.23	6.47	n.d.
Porosity (%)	74	71	79	92[a]
Bed density ($g.mL^{-1}$)	0.12	0.12	0.12	n.d.
Bed density ($g.mL^{-1}$) [b]	0.115	0.137	0.125	0.321[b]
Skeletal density ($g.mL^{-1}$)	0.44	0.4	0.55	n.d.
Median pore aperture (nm)	2366	2052	2595	43[c]

Table S3. Mercury intrusion porosimetry data [a] value calculated from bed and TiO_2 densities, [b] value measured from the mass and volume of tested materials, and [c] value calculated from cubic close packing approximation considering bed density and average particles size of TiO_2 P25 of 21 nm.

Materials	TiO_2@Si(HIPE)			TiO_2 P25
	I	II	III	Powder
Bandgap energy (eV)	3.1	3.1	3.1	3.1
%wt TiO_2 content (%)	32	29	21	100
Anatase/Rutile ratio	100/0	60/40	100/0	80/20
Anatase crystallites size (nm)	7	6.4	12.1	31.1
Rutile crystallites size (nm)	n.a.	6.5	n.a.	19.2

Table S4. Diffuse reflectance UV/Visible spectroscopy, XRF and XRD data

Sample	l_t (m)	l_i (m)	A	B	Chi^2	n_eff	L (mm)	lt (µm)		
P25 TiO_2 powder								**3.1**	**±**	**0.3**
experiment #1	*3.47E-06*	*1.00E-03*	*7.99E-02*	*1.47E-04*	*1.69E-02*	*1.20*	*2.00*			
experiment #2	*2.84E-06*	*7.34E-04*	*7.99E-02*	*1.01E-04*	*1.21E-02*	*1.20*	*2.00*			
experiment #3	*2.85E-06*	*6.84E-04*	*7.95E-02*	*9.88E-05*	*2.31E-02*	*1.20*	*2.00*			
mean	3.05E-06	8.06E-04	7.98E-02	1.16E-04	1.74E-02					
standart deviation	2.78E-07	1.29E-04	1.78E-04	2.09E-05	3.82E-03					
TiO_2@Si(HIPE)										
I								**20.1**	**±**	**1.3**
experiment #1	*1.92E-05*	*6.01E-04*	*3.87E-02*	*4.63E-03*	*1.51E-01*	*1.06*	*8.47*			
experiment #2	*1.91E-05*	*6.88E-04*	*3.92E-02*	*5.29E-03*	*5.64E-01*	*1.06*	*8.47*			
experiment #3	*2.20E-05*	*6.75E-04*	*3.85E-02*	*4.78E-03*	*7.37E-02*	*1.06*	*8.47*			
mean	2.01E-05	6.55E-04	3.88E-02	4.90E-03	2.63E-01					
standart deviation	1.27E-06	3.58E-05	2.67E-04	2.60E-04	2.00E-01					
II								**16.0**	**±**	**0.6**
experiment #1	*1.65E-05*	*8.41E-04*	*2.06E-02*	*9.00E-04*	*5.77E-02*	*1.05*	*3.50*			
experiment #2	*1.65E-05*	*8.45E-04*	*2.06E-02*	*6.88E-04*	*1.09E-01*	*1.05*	*3.50*			
experiment #3	*1.51E-05*	*9.80E-04*	*2.06E-02*	*9.04E-04*	*4.32E-02*	*1.05*	*3.50*			
mean	1.60E-05	8.89E-04	2.06E-02	8.31E-04	6.98E-02					
standart deviation	6.22E-07	6.09E-05	0.00E+00	9.51E-05	2.58E-02					
III								**25.6**	**±**	**1.1**
experiment #1	*2.39E-05*	*1.59E-03*	*4.13E-02*	*6.93E-04*	*8.57E-02*	*1.04*	*5.00*			
experiment #2	*2.56E-05*	*1.95E-03*	*4.15E-02*	*5.12E-04*	*2.83E-02*	*1.04*	*5.00*			
experiment #3	*2.72E-05*	*2.77E-03*	*6.79E-02*	*1.60E-04*	*5.60E-03*	*1.04*	*5.00*			
mean	2.56E-05	2.10E-03	5.02E-02	4.55E-04	3.99E-02					
standart deviation	1.11E-06	4.44E-04	1.18E-02	1.97E-04	3.06E-02					

Table S5. Photonic simulation results for each considered sample

Parameters	Column A	Column B	Column C	Column D
Detectable gases	H_2, O_2, N_2, CH_4, CO	Air, N_2, CH_4, CO	CH_4, CO_2, C_2H_4, C_2H_6, C_3H_6, C_3H_8, C_3H_4	C_3H_6, C_3H_8, C_3H_4, C_4H_{10}, C_4H_6, C_5H_{12}
Column type	MS5A	MS5A	PLOTQ	OV1
Dimensions	10 m x 0.32 mm	10 m x 0.32 mm	10 m x 0.32 mm	14 m x 0.32 mm
Injection temperature (°C)	50	50	70	50
Column temperature (°C)	50	70	60	40
Injection time (ms)	100	100	50	50
Backflush time (s)	4	4	-	-
Column pressure (psi)	28	28	25	25
Carrier gas	Argon	Helium	Helium	Helium

Table S6. µGC-TCD analysis parameters for CO_2 valorization test monitoring

Column	Quantified gases	Retention times (s)
A	H_2	39.4
	O_2	50.5
	N_2	64.8
B	CO	118.7
C	CH_4	23.6
	CO_2	25.1
	C_2H_6	40.0
	H_2O	96.1
	C_3H_8	138.1

Table S7: Retention time of quantified gases for the first three columns

Sample	h (mm)	$m_{catalyst}$ (g)	m_{TiO2} (g)	TiO_2 loading ($kg.m^{-2}$)	r_{e-} ($mol.s^{-1}$)	r_{e-} ($\mu mol.h^{-1}.m^{-2}$)	r_{e-} ($\mu mol.h^{-1}.g_{TiO2}^{-1}$)	Selectivities (%)			
								H_2	CO	CH_4	C_2H_6
P25 TiO_2 powder											
	0.21	0.04	0.04	0.07	3.29E-11	223	3.31	29	12	48	10
	0.36	0.06	0.06	0.12	4.62E-11	313	2.71	53	3	30	12
	0.65	0.11	0.11	0.21	2.97E-11	202	0.97	48	11	30	11
	1.00	0.17	0.17	0.32	1.37E-11	93	0.29	46	40	8	4
TiO_2@Si(HIPE)											
I	2.0	0.18	0.06	0.07	1.56E-10	697	9.47	0	0	90	10
	2.7	0.25	0.08	0.10	2.35E-10	1050	10.57	4	1	86	7
	3.0	0.28	0.09	0.11	2.53E-10	1134	10.27	0	0	78	22
	4.0	0.37	0.12	0.15	3.16E-10	1416	9.62	1	1	85	13
II	3.0	0.33	0.10	0.12	3.46E-11	155	1.30	8	0	85	11
	4.0	0.44	0.13	0.16	4.09E-11	183	1.15	16	0	76	7
	5.0	0.55	0.16	0.20	5.23E-11	234	1.18	18	0	77	4
	6.0	0.66	0.19	0.24	6.34E-11	284	1.19	16	8	70	6
	7.0	0.77	0.22	0.28	5.18E-11	232	0.83	7	8	80	5
	8.0	0.88	0.26	0.32	4.47E-11	200	0.63	7	8	71	12
	9.0	0.99	0.29	0.36	4.41E-11	197	0.55	15	8	68	8
III	3.0	0.30	0.06	0.08	3.04E-11	136	1.73	8	21	71	0
	4.0	0.40	0.08	0.11	3.62E-11	162	1.55	9	18	73	0
	6.0	0.60	0.13	0.16	5.27E-11	236	1.50	4	5	87	4
	7.0	0.70	0.15	0.18	4.82E-11	216	1.17	3	10	78	9

Table S8: Photocatalytic tests results for each considered sample. When the sum of selectivities does not reach 100%, this indicates traces of C_3 products

Materials	k_0 ($mol^{-1}.h^{-1}$)	K (mol^4)	α (m^{-1})
P25 TiO_2 powder	4.27E+16	5.62E-76	522
TiO_2@Si(HIPE)			
I	2.15E+15	9.35E-71	16
II	1.80E+14	3.34E-70	26
III	4.59E+14	2.77E-70	12

Table S9: Model best parameters k_0, K and α fitted with experimental data, finding a single value for *n* being 16.